Materials Today • Volume xxx, Number xx • xxxx 2018 RESEARCH

ELSEVIER

RESEARCH: Original Research

Dynamic regulating of single-mode lasing in ZnO microcavity by piezoelectric effect

Junfeng Lu [1,2], Zheng Yang [1,2], Fangtao Li [1], Mingming Jiang [3], Yufei Zhang [1], Junlu Sun [1], Guofeng Hu [1,2], Qian Xu [1,2], Chunxiang Xu [4], Caofeng Pan [1,2,*], Zhong Lin Wang [1,2,5,*]

[1] CAS Center for Excellence in Nanoscience, Beijing Key Laboratory of Micro-nano Energy and Sensor, Beijing Institute of Nanoenergy and Nanosystems, Chinese Academy of Sciences, Beijing 100083, PR China
[2] School of Nanoscience and Technology, University of Chinese Academy of Sciences, Beijing 100049, PR China
[3] State Key Laboratory of Luminescence and Applications, Changchun Institute of Optics, Fine Mechanics and Physics, Chinese Academy of Sciences, Changchun 130033, PR China
[4] State Key Laboratory of Bioelectronics, School of Biological Science and Medical Engineering, Southeast University, Nanjing 210096, PR China
[5] School of Materials Science and Engineering, Georgia Institute of Technology, Atlanta, GA 30332-0245, USA

Realizing single-mode-lasing output while being able to dynamically select and regulate a specified resonant mode could bring revolutionary impact for laser technology, on-chip data communication, and optical sensing/switches. Here, we demonstrate a single-mode lasing achieved by the piezoresistive and piezoelectric polarization synergistic effect on an epoxy-encapsulated ZnO microresonator. Based on relative shifts of gain spectrum and the resonant wavelength, the lasing mode in a hexagonal ZnO rod can be selected and regulated dynamically within a certain range. The relationship between the corresponding applied strain and the tunable refractive index is analyzed in depth and discussed systematically. Our studies open up exciting avenues for constructing optical mode-phase modulator, high-sensitive optical switches and color-perceived optical sensing.

Introduction

Since A. Einstein proposed the theory of stimulated emission in 1917 [1], the development of lasers has drawn much attention due to their vast applications in defense, medical treatment, and communication technology. The traditional laser cavities can confine and select a large number of resonant modes by utilizing the confining dimension of the cavity [2–5]. Laser emission at multiple frequencies will not only result in the group-velocity dispersion-induced temporal pulse broadening and false signaling, but also be subject to mode competition-dependent random fluctuations and instabilities. Achieving the stable single-mode lasing output is an effective strategy to avoid these series of problems, which is also of fundamental importance for various scientific and technological applications. In the last few decades, much effort has been devoted to enforcing single-mode operation, such as the construction of distributed Bragg reflector (DBR) mirrors or distributed feedback (DFB) gratings [6–8], reduction of cavity size for enlarging free spectral range (FSR) [9–11], coupled-resonant cavities through Vernier effect [12–14], spatially varied optical pumping [15,16], and parity-time symmetry breaking [17–19]. However, these approaches are applicable to pre-designed cavity configurations and highly rely on complex microfabrication technology. Also, reducing the cavity size to expand the FSR will suppress the acquisition of optical gain, which not only leads to the increase in optical loss, but also causes the increase in lasing threshold. Therefore,

* Corresponding authors at: CAS Center for Excellence in Nanoscience, Beijing Key Laboratory of Micro-nano Energy and Sensor, Beijing Institute of Nanoenergy and Nanosystems, Chinese Academy of Sciences, Beijing 100083, PR China (C. Pan). School of Materials Science and Engineering, Georgia Institute of Technology, Atlanta, GA 30332-0245, USA (Z.L. Wang).

E-mail addresses: Pan, C. (cfpan@binn.cas.cn), Wang, Z.L. (zhong.wang@mse.gatech.edu).

1369-7021/© 2018 Elsevier Ltd. All rights reserved. https://doi.org/10.1016/j.mattod.2018.12.001

Please cite this article in press as: J. Lu et al., Materials Today (2018), https://doi.org/10.1016/j.mattod.2018.12.001

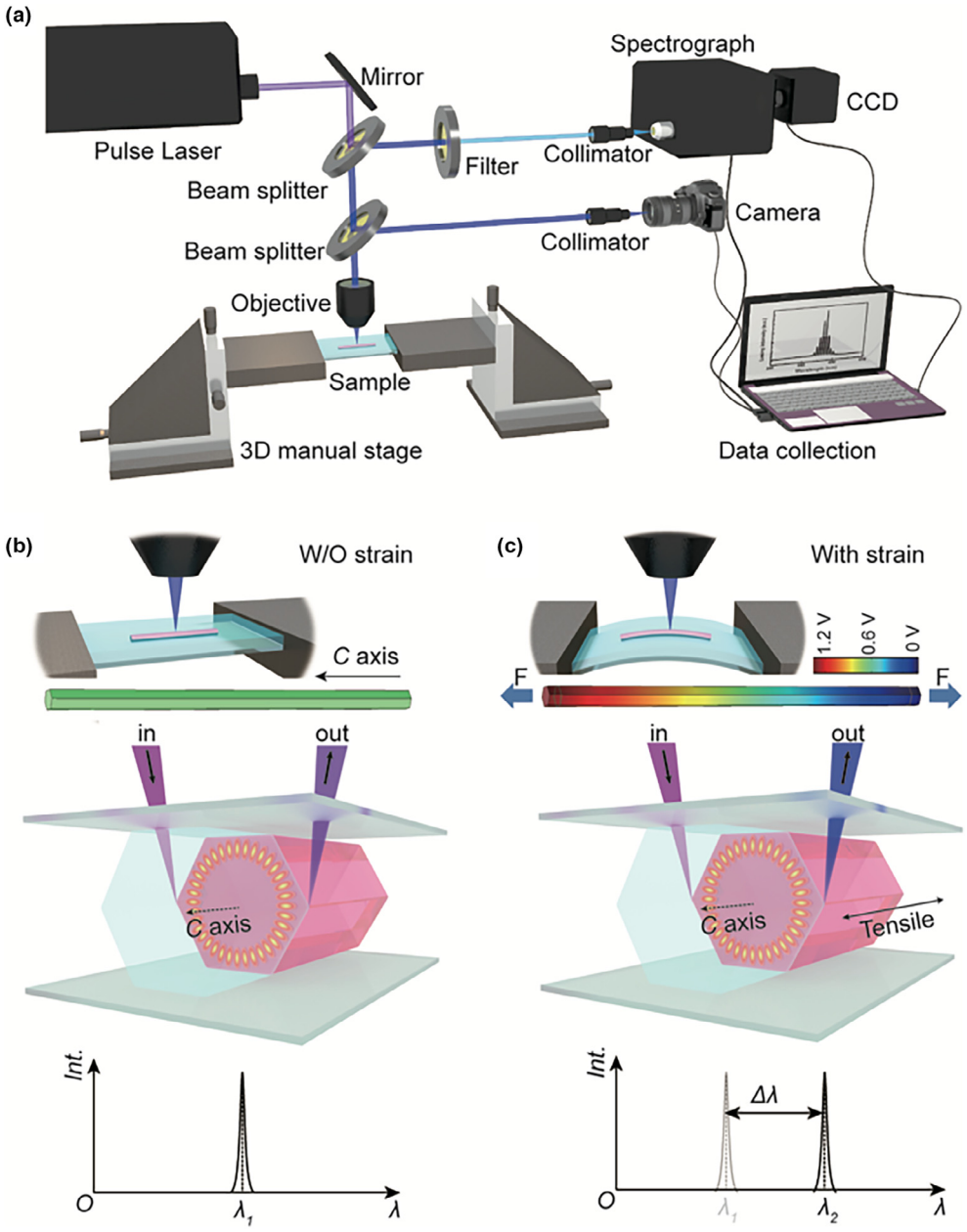

FIGURE 1

Optical path system and proposed mechanism for dynamic modulating lasing mode in ZnO microcavity. (a) The entire optical path diagram. (b) Schematic view of the excited WGMs in ZnO microcavity without applied strain by a focused Nd:YAG laser. The lasing wavelength is assumed to be at λ_1 (purple light). (c) Schematic view of the excited WGMs in ZnO microcavity under an applied tensile strain along the *c* axis, where the lasing mode will redshift from λ_1 to λ_2 (blue light). Piezopotential distribution in a ZnO microrod is simulated by a finite-element analysis method (COMSOL).

it is urgent to develop a simple method to achieve single-mode lasing and realize the regulation of lasing mode dynamically.

Previous explorations on the piezoresistive effect and piezoelectric polarization effect dependence of optical bandgap [20–22] and refractive index [23,24] offers a practicable strategy for dynamically tuning gain region and mode position, which is expected to realize lasing mode modulation. ZnO is an ideal gain medium for designing UV laser devices [25–28] because of its wide direct bandgap (3.37 eV) and high exciton binding energy (60 meV). In addition, the non-centrosymmetric hexagonal wurtzite ZnO micro/nanostructures not only provide a natural configuration for optical oscillations [29–32], but also offer a theoretical support for the existence of the piezoelectric polarization effect under mechanical perturbations [33–36]. As early as 1967, Vedam et al. [23] reported the effect of the pressure-induced polarizability on refractive index is greater than that caused by the increased number of dispersion centers per unit volume in the wurtzite-structural crystals, opening a door to dynamically modulate the lasing mode by utilizing the piezoelectric polarization effect. Combined with the method of controlling lasing mode output through reducing the resonator size to modulate the FSR, it is expected to obtain single-mode lasing while

Please cite this article in press as: J. Lu et al., Materials Today (2018), https://doi.org/10.1016/j.mattod.2018.12.001

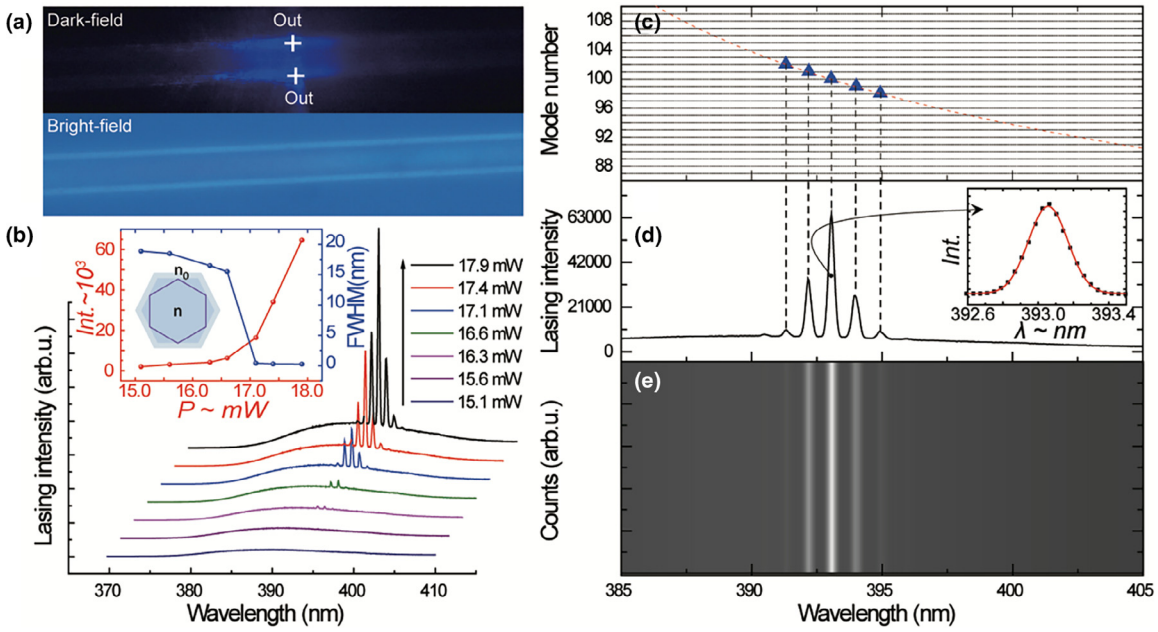

FIGURE 2

Mode analysis. (a) The physical photograph and bright/dark-field optical image of the excited ZnO microrod. (b) Lasing spectra of the measured ZnO microcavity under different pumping power, Inset: input–output characteristic, power-dependent FWHM and the schematic diagram of whispering-gallery mode in ZnO microcavity. (c) Comparison of the calculated (blue triangle) and experimental (dash line) mode wavelength. (d, e) lasing spectrum and mapping at the pumping power of 17.9 mW. Insets shows single lasing peak fitting by Gaussian function.

enabling to realize the dynamic modulation and selection based on the piezoresistive and piezoelectric polarization synergy effect, which avoids the use of submicron-sized cavities, thereby avoiding the poor optical field confinement and serious energy loss.

Here, we designed several individual ZnO microresonators with different dimensions encapsulated by epoxy resin and fixed on the flexible PET (Polyethylene terephthalate) substrate. The dependence of FSR and Q-factor on the cavity size were analyzed and discussed systematically. Experimental and theoretical simulation results demonstrated that the cavity size reduction will result in the decreasing of optical-field confinement capacity, the resonant mode number, and the increasing of free spectral range. Exploiting the modulation of the piezoresistive and piezoelectric polarization effect on the gain region and refractive index, the desired single-mode obtained from a micro-sized ZnO resonator with a diameter of ~1.7 μm can be selected and regulated dynamically in a range of 9.3 nm. Consequently, our approach naturally exhibits the capacity of dynamic selection and modulation for single-mode lasing output while ensuring lasing quality.

Material and methods

Fabrication of the samples

ZnO microrods were synthesized by a simple vapor-phase transport method as our previous reports [37]. Some individual ZnO microrods with different diameters were picked out and placed on a flexible PET substrate, fixed by Kapton tape initially. Then, the probe was used to pick up a microdroplet of epoxy resin glue, a mixture of epoxy resin and hardener with mass ratio of 2:1. Finally, these separate ZnO microrods were packaged by the high transparent epoxy resin glue with a refractive index (n_0) of ~1.58 through a spin coating method.

Optical setup

To measure the lasing characteristics under different cases, a Nd: YAG laser (λ_{ex} = 355 nm, repetition rate 1000 Hz, pulse length 50 ns) coupled with a confocal μ-PL system (Zeiss M1) was employed as an excitation source. The light emission was detected and analyzed by a CCD detector and an optical multichannel analyzer (Andor, SR-500i-D1-R) with a 1200 g/mm grating. The applied strain was manifested by the deformation of the flexible PET substrate manipulated by a manual three-dimensional displacement stage. The physical photograph of the measurement setup can be seen in Figure S11 of Supporting Information.

Simulation

To investigate the mode evolution with decreasing of ZnO microrod diameters, the Finite Difference Time Domain (FDTD) software was employed to calculate the near-field electric field distribution of the fundamental mode confined in ZnO microcavity with different diameters. The refractive index of ZnO is 2.5 at λ = 385 nm. The diameters of ZnO microcavities were 10 μm, 6 μm, 4 μm, 2 μm and 1.5 μm, respectively.

Results and discussion

The wurtzite hexagonal ZnO microrods fabricated by vapor-phase transport method possess the advantages of good crystallinity and high optical quality. It is a typical active resonator, not only offering the suitable configuration for light

Please cite this article in press as: J. Lu et al., Materials Today (2018), https://doi.org/10.1016/j.mattod.2018.12.001

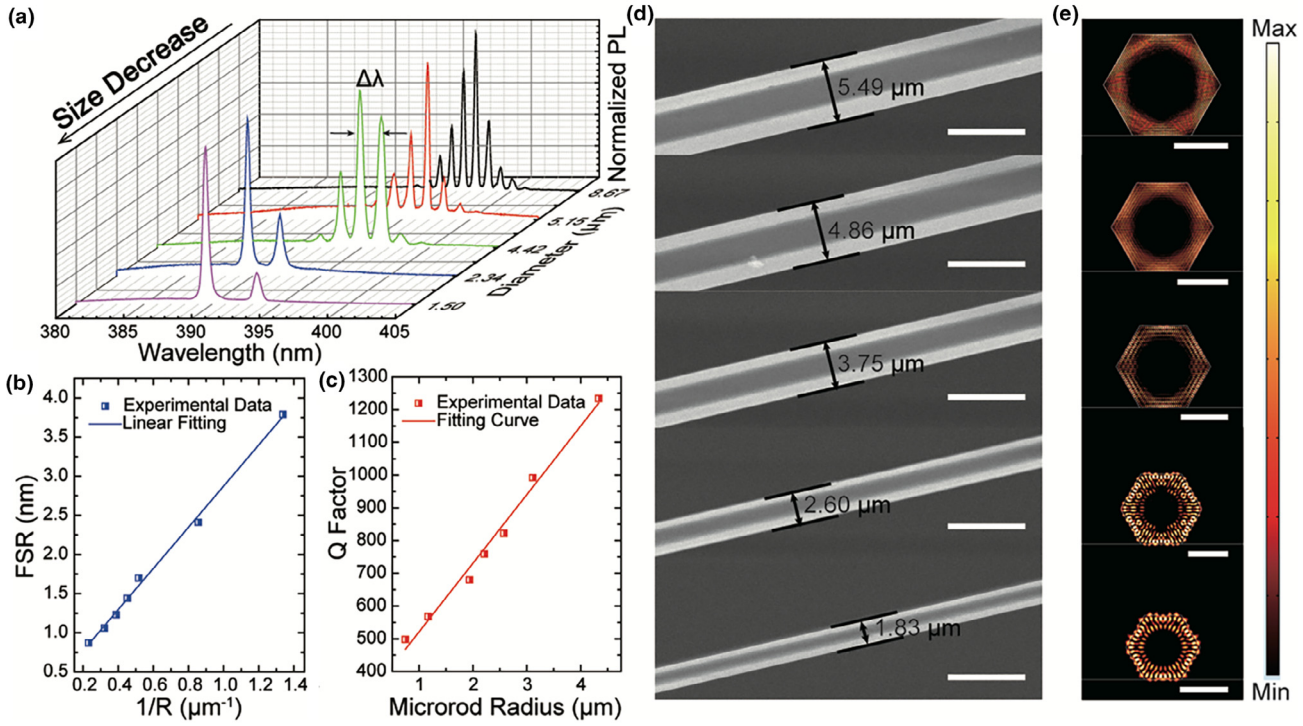

FIGURE 3

Size-dependent lasing characteristics and simulated results. (a) Lasing spectra collected from different sizes of ZnO microcavities. (b, c) Dependence of free spectral range (FSR) and quality factor (Q) on ZnO microrod radius. (d) SEM images of ZnO microrods with different diameters. Scale bar is 6 μm. (e) Electrical-field distribution of the fundamental mode in *x*-*y* plane from different ZnO microcavities. Scale bars: 5 μm, 3 μm, 2 μm, 1 μm, and 1 μm, respectively.

amplification, but also providing sufficient optical gain to compensate the loss during light propagation. In addition, due to its non-centrally symmetric wurtzite structure of ZnO, straining its basic unit cell will result in the polarization of the cations and anions in the crystal, and leading to the change of refractive index of the optical resonator [23]. Based on this idea, we proposed an efficient approach to dynamically modulate coherent light emission and mode-phase. Figure 1a shows a complete set of confocal micro-system coupled with a Nd:YAG 355 nm laser, a spectrograph equipped with a CCD detector and image capture system, which can be used to investigate the optical properties of the encapsulated ZnO microresonators under different applied strains. Two three-dimensional manual displacement stages were used to refocus and apply the strain on the microresonators. Figure 1(b, c) show the schematic view of the excited WGMs (whispering-gallery modes) in ZnO microcavity without and with the external mechanical strain. When the ZnO microcavity is under tensile strain, the anions and cations inside the crystal are polarized, so a piezopotential is created at both ends of ZnO microrod, as shown in the simulation results of Figure 1c (the upper panel). The generated piezoelectric polarization effect under externally applied strain can be used to tune the refractive index of ZnO microresonator flexibly, thereby achieving the purpose of dynamic regulation of lasing mode output, as illustrated in the lower panel of Figure 1c.

Figure 2a shows the physical photograph of the measurement setup and bright/dark-field optical image of the excited microresonator. Figure 2b shows the typical lasing spectra *versus* the pumping power in an encapsulated ZnO microresonator with a diameter of ~6.6 μm. At a low pumping power of 15.1 mW, a weak and broad emission peak centered at $\lambda = 389.37$ nm can be observed, which is attributed to ZnO intrinsic spontaneous emission. As the pumping power increases to 16.6 mW, some discrete narrow peaks emerge in the region of ZnO NBE (near-band edge) emission, which indicates that the lasing threshold is ~16.6 mW. When the pumping power further increases to 17.9 mW, the lasing intensity also increases dramatically, suggesting the transformation of the excitonic recombination from spontaneous transition to stimulated transition. The inset of Figure 2b plots the integrated PL intensity and FWHM (full width at half maximum) as a function of the pumping power. A typical transition point at pumping power of ~16.6 mW can be observed, where the lasing intensity and FWHM will dramatically increase and decrease, respectively, with further increasing of pumping power. It is noteworthy that the ZnO microresonator wrapped by epoxy resin still maintains a high Q factor of 1455, which can be estimated according to $Q = \lambda/\Delta\lambda$, where λ and $\Delta\lambda$ are the wavelength and FWHM of the lasing peak, respectively. To further analyze the selection of the lasing mode by utilizing the encapsulated ZnO microresonator, the plane wave model for hexagonal WGM cavity has been used. According to Fresnel formula, the relationship of mode serial number (N) and the corresponding resonant wavelength λ for the microcavity exposed to the air with the refractive index of ~1 can be expressed as Eq. S2 (see Eq. S2 in Supporting Information). However, in our case, the ZnO microcavity was wrapped by an epoxy resin (see Figure S2 in Supporting Information) with a refractive index of $n_0 = 1.58$. Therefore, equation S2 should be modified into

Please cite this article in press as: J. Lu et al., Materials Today (2018), https://doi.org/10.1016/j.mattod.2018.12.001

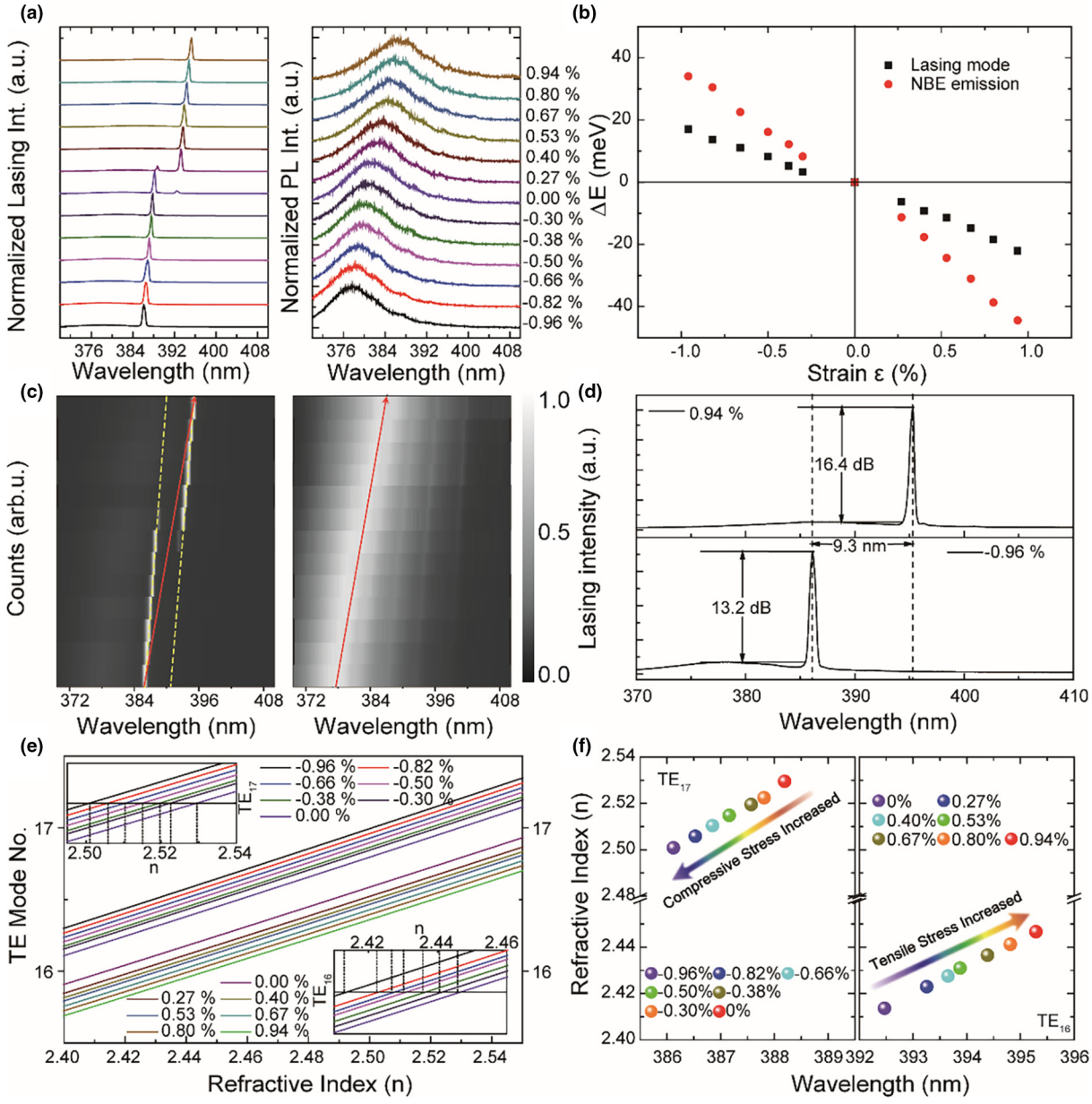

FIGURE 4

Achieving single-mode lasing and its dynamic regulation. (a) Spectra and (c) mapping of stimulated and spontaneous emission for the as-prepared microresonator under different degrees of compressive and tensile strain. (b) The blue-/red-shift variation for the NBE emission and lasing mode photon energy as a function of the compressive and tensile strain, respectively. (d) Comparison of single-mode lasing characteristics at a compressive strain of −0.96% and a tensile strain of 0.94%. (e) Refractive index of the TE_{17} and TE_{16} mode under different cases, namely, compressive and tensile strains. (f) The relationship of the resonant wavelength for TE_{17} and TE_{16} mode with refractive index under different compressive and tensile strains.

equation S3 (see Eq. S3 in Supporting Information), where $n_r = n/n_0$, n_r is the relative index of refraction, n and $n_0$are the refractive index of ZnO and epoxy resin, respectively. Based on Eq. S3, the TE mode number N can be calculated from 98 to 102, which was plotted as the blue triangles shown in Figure 2c. The calculated resonant wavelengths of the different modes matched well with the experimental one collected from the lasing spectrum in Figure 2(d, e), which is listed in Table S1 (see Table S1 in Supporting Information).

To gain more insights into the lasing characteristics, the lasing spectra with different diameters ranging from ~8.67 μm to ~1.50 μm have been measured, as shown in Figure 3a. It can be seen that the number of resonant mode decreases with size reduction of the microcavity in the gain region, which also means the increasing of the mode spacing ($\Delta\lambda$), namely, the free spectral range (FSR). As well known, the mode spacing and Q-factor depend on the size of the optical microresonator. As shown in Figure 3b, the mode spacing can be well-fitted by linear function, suggesting that the FSR is proportional to the inverse of the microcavity radius according to $\Delta\lambda = \lambda^2/L(n - \lambda dn/d\lambda)$, where $L = 3\sqrt{3}D/2$ is the path length of a round trip for hexagonal WGM cavity, D is the diameter of the microresonator, n is

Please cite this article in press as: J. Lu et al., Materials Today (2018), https://doi.org/10.1016/j.mattod.2018.12.001

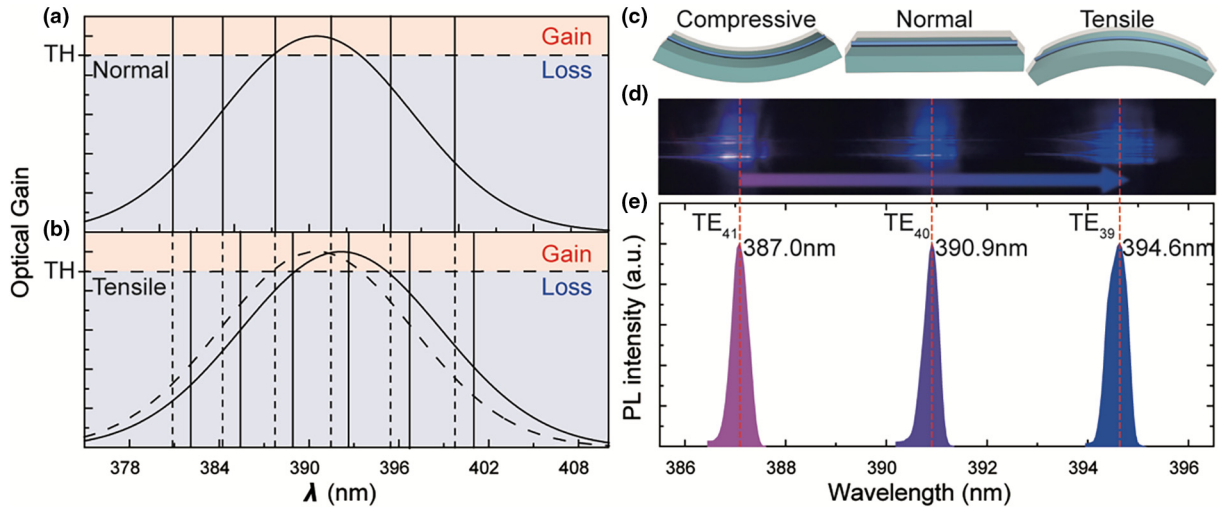

FIGURE 5

The mechanism analysis. The gain spectra and lasing mode positions at the normal (a) and tensile (b) states. Dark-field light emission photos (d) and lasing spectra (e) under different cases of compression, normal and tension (c), respectively.

the refractive index of ZnO, and $dn/d\lambda$ denotes the dispersion relation, the item of $(n - \lambda dn/d\lambda)$ represents the effective refractive index of ZnO. In addition, the Q-factor demonstrates the linear relation with the ZnO microresonator size shown in Figure 3c, which can be calculated by $Q = \lambda/\delta\lambda$, where λ and $\delta\lambda$ are the wavelength and FWHM of the resonant mode. It is reasonable because the smaller microcavity will lead to the weaker capability to confine the optical field, accompanied by the increasing of optical loss. To further analyze the effects of cavity size on lasing characteristics, the cross-sectional electric field distribution in ZnO microcavities with different sizes were calculated by a FDTD method, as shown in Figure 3e. Figure 3d shows SEM images of five representative ZnO microrods with the diameters ranging from 1.83 μm to 5.49 μm. The smooth surface of the microcavity provides a necessary condition for the total internal reflection of light waves at the ZnO/air interface. The simulation results demonstrate that the electric field of the fundamental mode is effectively confined in the bigger cavity, and presents multi-layer distribution inwardly along the edge of the cavity. As the cavity size reduces to 1.5 μm, the confinement effect of the cavity on the electric field is obviously weakened, and the number of the distributed layers inward along the edge of the cavity decreases, indicating the reduction of the lasing mode number, which is in good agreement with the experimental results. It should be possible to obtain single-mode lasing in a smaller ZnO microrod, as mentioned in the previous report [10]. Therefore, it is a feasible approach to regulate the lasing mode and realize the single-mode lasing by changing the size of the optical microresonator. However, a further reduction in cavity size will cause more severe radiation loss, resulting in low Q-factor and high lasing threshold. Thus, these important scientific issues need to be desperately solved.

In order to ensure the relatively high Q-factor, a ZnO microrod with a diameter of ~1.7 μm was selected as an optical microresonator. Utilizing the piezoelectric effect of ZnO, the wavelength of the resonant mode can be modulated dynamically, as shown in left panel of Figure 4a. In addition, the wavelength of near-band-edge emission also can be adjusted through the strain-induced energy bandgap variation, as shown in right panel of Figure 4a. To estimate the applied strain, the calculated model has been proposed (see Figure S3 in Supporting Information). When the tensile strain is applied from 0% to 0.94%, the redshift phenomenon appears in both the lasing peak and NBE emission peak. In contrast, an obviously blueshift of the lasing peak and NBE emission peak can be observed as the compressive strain increases from 0% to −0.96%. When the strain is 0%, two distinct lasing modes of TE_{17} and TE_{16} emerge with the pumping power (18.9 mW) in excess of the lasing threshold of 16.6 mW (see Figure S6 in Supporting Information). The wavelength for determining the modes (TE17 and TE16) is the experimental parameters of 388.20 and 392.47 nm, respectively. As the tensile strain is applied to 0.27%, the lasing intensity of TE_{17} decreases, while the lasing intensity of TE_{16} increases. When the applied tensile strain further increases, the single-mode lasing is obtained accompanied by the disappearance of TE_{17} mode. The wavelength of TE_{16} can be tuned from 392.47 nm to 395.36 nm with the tensile strain varying from 0% to 0.94% (see Figure S5 in Supporting Information). On the contrary, the applied compressive strain will lead to the blueshift of the lasing peak. When the compressive strain increases from 0% to −0.96%, the wavelength of lasing mode TE_{17} will be regulated from 388.20 nm to 386.06 nm (see Figure S5 in Supporting Information). In comparison, the wavelength variation rate of NBE emission peak with increasing of the applied strain is greater than that of lasing peak shown in Figure 4b, indicating the difference of the underlying mechanisms leading to the spectral evolution. In addition, according to the Poisson ratio of ZnO (~0.35), the decreased amount of D can be estimated as 1.61 nm, 2.38 nm, 3.15 nm, 3.99 nm, 4.76 nm, and 5.59 nm under the tensile strain of 0.27%, 0.40%, 0.53%, 0.67%, 0.80%, and 0.94%, respectively. The increased amount of D can be estimated as 1.79 nm, 2.26 nm, 2.98 nm, 3.93 nm, 4.88 nm, and 5.71 nm under the

Please cite this article in press as: J. Lu et al., Materials Today (2018), https://doi.org/10.1016/j.mattod.2018.12.001

compressive strain of −0.30%, −0.38%, −0.50%, −0.66%, −0.82%, and −0.96%, respectively. If only considering the change of the cavity, the trend of mode wavelength under different strain can be calculated as shown in Table S1, which is contrary to the observed experimental results. Therefore, the main factor leading to mode redshift is attributed to the change of refractive index caused by stress induced crystal polarization, while the redshift of PL is caused by the piezoresistive effect. The angular-dependent lasing spectra (see Figure S4 in Supporting Information) further confirm that the externally applied strain has little effect on the refractive index of the encapsulant, which is not enough to cause lasing mode shift. To clearly demonstrate the difference of these two cases, mappings of stimulated and spontaneous emission for the as-prepared microresonator under different degrees of compressive and tensile strain are given in Figure 4c. The yellow dashed lines represent the trend of resonant mode TE_{17} and TE_{16} wavelength with the variation of applied strain. The red arrowhead in the left panel of Figure 4c denotes the envelope of the lasing mode, whose slope corresponds to the trend of NBE emission wavelength, is shown in the right-hand panel. It suggests that the underlying mechanisms leading to the shift of the resonant mode and optical gain region are different in nature. Just because of the distinction, it provides a possibility for the resonant mode selection, single-mode lasing realization, and mode-phase dynamic modulation. Through the mode selection and dynamic regulation, a range of up to 9.3 nm for the single-mode lasing can be obtained, as shown in Figure 4d. The side-mode suppression ratio (SMSR) can be calculated as 16.4 dB and 13.2 dB in the cases of the tension and compression shown in Figure 4d, respectively, according to $SMSR = 10\log(M_1/M_2)$, where M_1 and M_2 are the intensity of the dominant mode and side mode. To further verify the piezoelectric polarization effect tuned refractive index of ZnO, the mode number of the lasing peaks can be identified with a diameter of ~1.7 μm in the strain-free case, based on Eq. S2. Then, the refractive index of the TE_{17} and TE_{16} mode under different degrees of applied strain can be calculated by fixing the value of the diameter (D), mode number (N), and the resonant wavelength (λ), as shown in Figure 4e. Also, the dependence of the refractive index on the applied strain for the TE_{17} and TE_{16} mode is shown in Figure S5, implying the greater effect of piezoelectric polarization on the refractive index than stain-induced varying of dispersion centers. In addition, Figure 4f plots the resonant wavelength of TE_{17} and TE_{16} as a function of refractive index under different compressive and tensile strains, respectively. The linear fitting results shown in Figure S5 present the greater impact of the piezoelectric polarization effect on the refractive index at the resonant frequency closed to the bandgap energy, clarifying the dominant reason for the change in refractive index distinctly. The similar optical phenomenon also can be obtained in different microresonators with diameters of ~5.1 μm and ~2.6 μm, demonstrating that it is an effective and universal method to dynamically modulate the coherent light emission, as shown in Figures S7 and S8. Meanwhile, in the wrapped-free ZnO microresonators, the single-mode lasing output also can be realized and tuned by applying tensile strain, as shown in Figure S9, which is similar to the results of the encapsulated one.

To deeply analyze the strain-induced mode selection, single-mode lasing realization and dynamic modulation, a summarized sketch of gain spectra and lasing mode positions at the normal and tensile states is drawn in Figure 5(a, b). In the normal case of Figure 5a, the solid Gaussian curve is the gain spectrum of ZnO with the WGM modes of the corresponding microresonator marked as the solid vertical lines and the lasing threshold denoted as the dashed black horizontal line. Only the modes that exceed the threshold value will be amplified and selected (red vertical line). As the tensile strain is applied, the redshift of the gain spectrum and the resonant wavelength will occur, as shown in Figure 5b. The dashed Gaussian curve and vertical lines are the initial state, while the solid ones represent the tensile state. Due to slower redshift speed of lasing mode, only one mode is located in the gain region, which will be amplified and selected marked with a solid red line. Finally, the single-mode lasing can be realized and tuned dynamically within a certain wavelength range. Not only that, it also provides a new method for flexible lasing mode selection and dynamic mode-phase regulation. Moreover, it also offers the possibility for rapid strain resolution by perceiving the color change of light emission ranging from 387.0 nm to 394.6 nm, as shown in Figure 5(c–e). The TE mode number of the dominant lasing peak regulates from 41 to 39 under three different cases of compression, normal and tension (see Figure S10 in Supporting Information). Because of the ultra-narrow linewidth of lasing mode, this method for strain-sensing has the characteristics of high sensitivity and high accuracy.

Conclusions

To summarize, the mode-optional and phase-modulated single-mode lasing have been achieved and tuned dynamically within a certain wavelength range based on an epoxy-encapsulated ZnO microresonator fixed on a flexible PET substrate. Piezoelectric polarization effect-induced change of refractive index enables the effective resonant wavelength of lasing mode modulation amplified and selected from the ZnO microcavity with an externally applied strain. Combined with strain-induced shift of gain spectrum, the single-mode lasing with different resonant modes of TE_{17} and TE_{16} can be exclusively selected and tuned within wavelengths from 386.06 nm to 395.36. SMSR at a tensile strain of 0.94% reaches up to 16.4 dB. As a result, this work paves the way in realizing of single-mode lasing without changing macroscopic ambient conditions, as well as providing new concept for turning mode-phase and selecting resonant mode dynamically with potential application in laser modulation, optical sensing/switches, photonic integrated circuit and optical communication encryption.

Acknowledgments

The authors thank the support of national key R&D project from Minister of Science and Technology, China (2016YFA0202703 and 2016YFA0202704), National Natural Science Foundation of China (No. 61805015, 51622205, 61675027, 51432005, 61505010 and 51502018), the China Postdoctoral Science Foundation Funded Project (No. 2018M630122), Beijing City Committee of Science and Technology (Z171100002017019 and Z181100004418004), Beijing Natu-

ral Science Foundation (4181004, 4182080, 4184110 and 2184131) and the "Thousand Talents" program of China for pioneering researchers and innovative teams.

Appendix A. Supplementary data

Supplementary data to this article can be found online at https://doi.org/10.1016/j.mattod.2018.12.001.

References

[1] A. Einstein, Phys. Z. 18 (1917) 121–128.
[2] X.X. Wang et al., ACS Nano 12 (2018) 6170–6178.
[3] J.Y. Xu et al., J. Am. Chem. Soc. 134 (2012) 12394–12397.
[4] P.F. Guo et al., Nano Lett. 13 (2013) 1251–1256.
[5] H. Zhou et al., ACS Nano 11 (2017) 1189–1195.
[6] H. Ghafouri-Shiraz, Distributed Feedback Laser Diodes and Optical Tunable Filters, Wiley, New York, 2003.
[7] D.C. Hanna et al., Electron. Lett. 8 (1972) 369–370.
[8] M.P. Nesnidal et al., IEEE Photonics Techol. Lett. 8 (1996) 182–184.
[9] R.M. Ma et al., Nat. Mater. 10 (2011) 110–113.
[10] J.T. Li et al., ACS Nano 9 (2015) 6794–6800.
[11] M.T. Hill et al., Nat. Photonics 1 (2007) 589–594.
[12] H.W. Gao et al., PNAS 110 (2013) 865–869.
[13] Y.Y. Wang et al., Nanoscale 8 (2016) 16631–16639.
[14] Y. Xiao et al., Nano Lett. 11 (2011) 1122–1126.
[15] S.F. Liew et al., Appl. Phys. Lett. 104 (2014) 231108.
[16] F.X. Gu et al., Light: Sci Appl. 6 (2017) e17061.
[17] H. Hodaei et al., Science 346 (2014) 975–978.
[18] L. Feng et al., Science 346 (2014) 972–975.
[19] B. Peng et al., Nat. Phys. 10 (2014) 394–398.
[20] X.W. Fu et al., ACS Nano 9 (2015) (1967) 11960–11961.
[21] B. Wei et al., Nano Lett 12 (2012) 4595–4599.
[22] X.B. Han et al., Adv. Mater. 21 (2009) 4937–4941.
[23] K. Vedam, T.A. Davis, Phys. Rev. 181 (1969) 1196–1201.
[24] W. Langer, J. Appl. Phys. 37 (1966) 3530–3532.
[25] J. Dai et al., Adv. Mater. 23 (2011) 4115–4119.
[26] S. Chu et al., Nat. Nanotechnol. 6 (2011) 506–510.
[27] H. Zhu et al., Adv. Mater. 21 (2009) 1613–1617.
[28] J.F. Lu et al., ACS Photonics 4 (2017) 2419–2424.
[29] M.H. Huang et al., Science 292 (2001) 1897–1899.
[30] C.X. Xu et al., Laser Photonics Rev. 8 (2014) 469–494.
[31] H. Cao et al., Phys. Rev. Lett. 82 (1999) 2278–2281.
[32] J.F. Lu et al., ACS Photonics 2 (2014) 73–77.
[33] Z.L. Wang, J.H. Song, Science 312 (2006) 242–246.
[34] Z.L. Wang, Adv. Mater. 19 (2007) 889–892.
[35] Z.L. Wang, Nano Today 5 (2010) 540–552.
[36] C.F. Pan et al., Nat. Photonics 7 (2013) 752–758.
[37] J.F. Lu et al., ACS Appl. Mater. Interfaces 6 (2014) 18301–18305.

Please cite this article in press as: J. Lu et al., Materials Today (2018), https://doi.org/10.1016/j.mattod.2018.12.001